AGU PUBLICATIONS

Geophysical Research Letters

RESEARCH LETTER
10.1002/2014GL062547

Key Points:
- Origin of seismic anisotropy and inferred mantle dynamics in subduction zones
- Natural documentation of olivine fabric across a paleolithosphere
- Transitional olivine fabric as source for shear wave splitting in mantle wedges

Supporting Information:
- Figures S1 and S2

Correspondence to:
J. Précigout,
jacques.precigout@univ-orleans.fr

Citation:
Précigout, J., and B. S. G. Almqvist (2014), The Ronda peridotite (Spain): A natural template for seismic anisotropy in subduction wedges, *Geophys. Res. Lett.*, *41*, doi:10.1002/2014GL062547.

Received 15 NOV 2014
Accepted 21 NOV 2014
Accepted article online 25 NOV 2014

The Ronda peridotite (Spain): A natural template for seismic anisotropy in subduction wedges

Jacques Précigout[1] and Bjarne S. G. Almqvist[2]

[1]Institut des Sciences de la Terre d'Orléans, UMR-CNRS 7327, Université d'Orléans, Orléans, France, [2]Department of Earth Sciences, Uppsala University, Uppsala, Sweden

Abstract The origin of seismic anisotropy in mantle wedges remains elusive. Here we provide documentation of shear wave anisotropy (AV*s*) inferred from mineral fabric across a lithosphere-scale vestige of deformed mantle wedge in the Ronda peridotite. As predicted for most subduction wedges, this natural case exposes a transition from A-type to B-type olivine fabric that occurs with decreasing temperature and enhanced grain boundary sliding at the expense of dislocation creep. We show that B-type fabric AV*s* (maximum of 6%) does not support geophysical observations and modeling, which requires 8% AV*s*. However, an observed transitional olivine fabric (A/B) develops at intermediate temperatures (800–1000°C) and can generate AV*s* ≥ 8%. We predict that the A/B-type fabric can account for shear wave splitting in contrasting subduction settings, exemplified by the Ryukyu and Honshu subduction wedges. The Ronda peridotite therefore serves as a natural template to decipher the mantle wedge deformation from seismic anisotropy.

1. Introduction

Elastic waves stem from the energy released during earthquakes, and they propagate through the Earth's interior at velocities that are directionally dependent on the state and properties of the surrounding rocks. In particular, upon entering an anisotropic medium, the elastic shear wave splits into two orthogonally polarized waves, consisting of fast (Vs_1) and slow (Vs_2) velocity components. At seismic stations, the geometry and magnitude of shear wave splitting are, respectively, recorded as the polarization direction of the fast shear wave (fast direction) and the time difference between the arrival of the fast and slow shear components (delay time). The delay time depends on both the degree of shear wave anisotropy ($AVs = 200(Vs_1 - Vs_2)/(Vs_1 + Vs_2)$) and thickness of the anisotropic layer [*Silver et al.*, 1999]. Measurement of shear wave splitting is a crucial diagnostic tool to interpret structures and flow dynamics in the out-of-reach mantle.

In most subduction zones, shear waves exhibit a general trend of fast directions that are polarized parallel to the trench in the fore-arc region and normal to the trench in the back-arc region. In contrast, delay times vary considerably from one subduction zone to another, ranging in average from 0.3 s in Japan or Sumatra to greater than 1 s in the Aleutians or Tonga [*Long and Silver*, 2008]. In the case of the low-delay-time subduction zone along Japan, *S* wave splitting has been attributed to the olivine fabric—or lattice-preferred orientation (LPO)—in the mantle wedge [*Nakajima and Hasegawa*, 2004; *Karato et al.*, 2008], where trench-parallel and trench-normal fast directions would likely be due to, respectively, flow-normal [100] axis LPO in the cold wedge (B-type fabric [*Mizukami et al.*, 2004]) and flow-parallel [100] axis LPO in the inner, hotter wedge (A-, E-, or C-type fabrics). However, from the mantle wedge geometry and seismic raypath azimuths in high-delay-time subduction zones, it can be inferred that B-type fabric requires approximately 9% AV*s* to account for the recorded delay times [*Kneller et al.*, 2008]; this value has been recently lowered to 8% based on detailed observations and modeling of the Ryukyu subduction system [*McCormack et al.*, 2013]. Previous measurements of olivine seismic anisotropy in laboratory and nature [*Jung and Karato*, 2001; *Skemer et al.*, 2006; *Tasaka et al.*, 2008] indicated that *S* wave anisotropy accounts for <7% for B-type fabric. As a consequence, although suitable to account for the geometry of fast directions in subduction zones, the strain-induced olivine fabric has been discarded in favor of other hypotheses [*Behn et al.*, 2007; *Long and Silver*, 2008; *Faccenda et al.*, 2008; *Katayama et al.*, 2009]. Here we provide a natural equivalent of mantle wedge deformation, where the olivine fabric itself can explain the observed shear wave splitting in subduction zones.

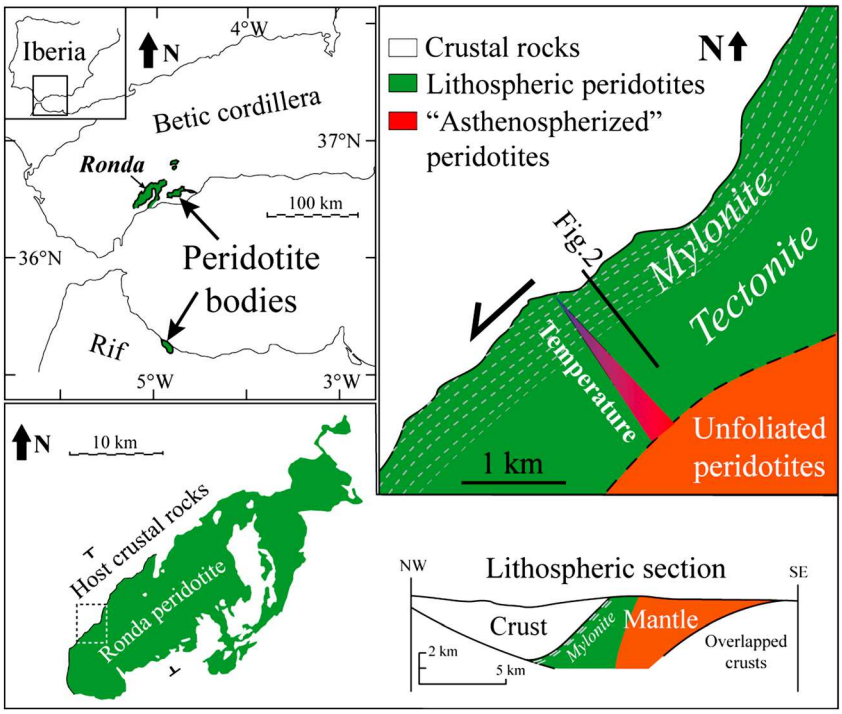

Figure 1. Maps and cross section of the Ronda massif and its northwestern structural domains, including a kilometer-scale shear zone of lithospheric mantle between an overlying paleocontinental crust and underlying asthenospherized mantle [*Van der Wal and Vissers*, 1993, 1996; *Vauchez and Garrido*, 2001; *Lenoir et al*., 2001]. The shear zone encompasses a domain of high-strain deformation that strengthens toward the peridotite/crust contact (mylonite) and its weakly deformed protolith (tectonite).

2. The Ronda Mantle Shear Zone

The Ronda massif belongs to the internal domain of the Betic Cordillera in southern Spain (Figure 1). It encompasses several lenses of subcontinental peridotites that were exhumed from the mantle wedge of the African subduction zone during the Cenozoic [*Van der Wal and Vissers*, 1993; *Garrido et al*., 2011]. As remnants of exhumation, several structural domains occur in the northwestern Ronda peridotite, which comprises (1) a 500 m thick mantle mylonite underlying a paleocontinental crust [*Balanyá et al*., 1997] and (2) a plurikilometer thick tectonite overlying an asthenospherized mantle section [*Van der Wal and Vissers*, 1996; *Vauchez and Garrido*, 2001]. These two structural domains are mostly composed of spinel-bearing peridotites and make up a kilometer-scale shear zone of lithospheric mantle coeval with a temperature gradient ranging from 1280°C (athenospherized section) to ~1000°C in the tectonite and then to ~850°C in the mylonite (Figure 1) [*Van der Wal and Vissers*, 1993; *Lenoir et al*., 2001]. The high-strain deformation in the mylonite originates from subcrustal viscous strain localization during back-arc continental extension [*Précigout et al*., 2007; *Garrido et al*., 2011; *Précigout et al*., 2013].

3. Olivine Fabric

Recently, the Ronda peridotite has been the subject of a detailed documentation of olivine LPO across the mantle shear zone, describing a progressive transition from A-type fabric in the tectonite to B-type fabric in the uppermost mylonite beneath the overlying crust (Figure 2a) [*Précigout and Hirth*, 2014]. Indeed, in the tectonite, the olivine LPO develops A-type fabric with the $[100]_a$ axis in the lineation, the $[010]_b$ axis normal to the foliation, and the $[001]_c$ axis normal to the lineation in the foliation plane [*Jung and Karato*, 2001]. However, whereas the *b* axis remains unchanged in the uppermost mylonite, the *a* and *c* axes rotate 90° with respect to the foliation pole, giving rise to a B-type fabric with the *c* axis parallel to the lineation (Figure 2b) [*Mizukami et al*., 2004]. The B-type fabric progressively overprints the A-type fabric over a section that is greater than 300 m thick within the mylonite, where LPOs develop a girdled pattern for both the *a* and *c* axes (A/B-type fabric) (Figure 2b) [*Précigout and Hirth*, 2014]. This A-type/B-type fabric transition occurs with

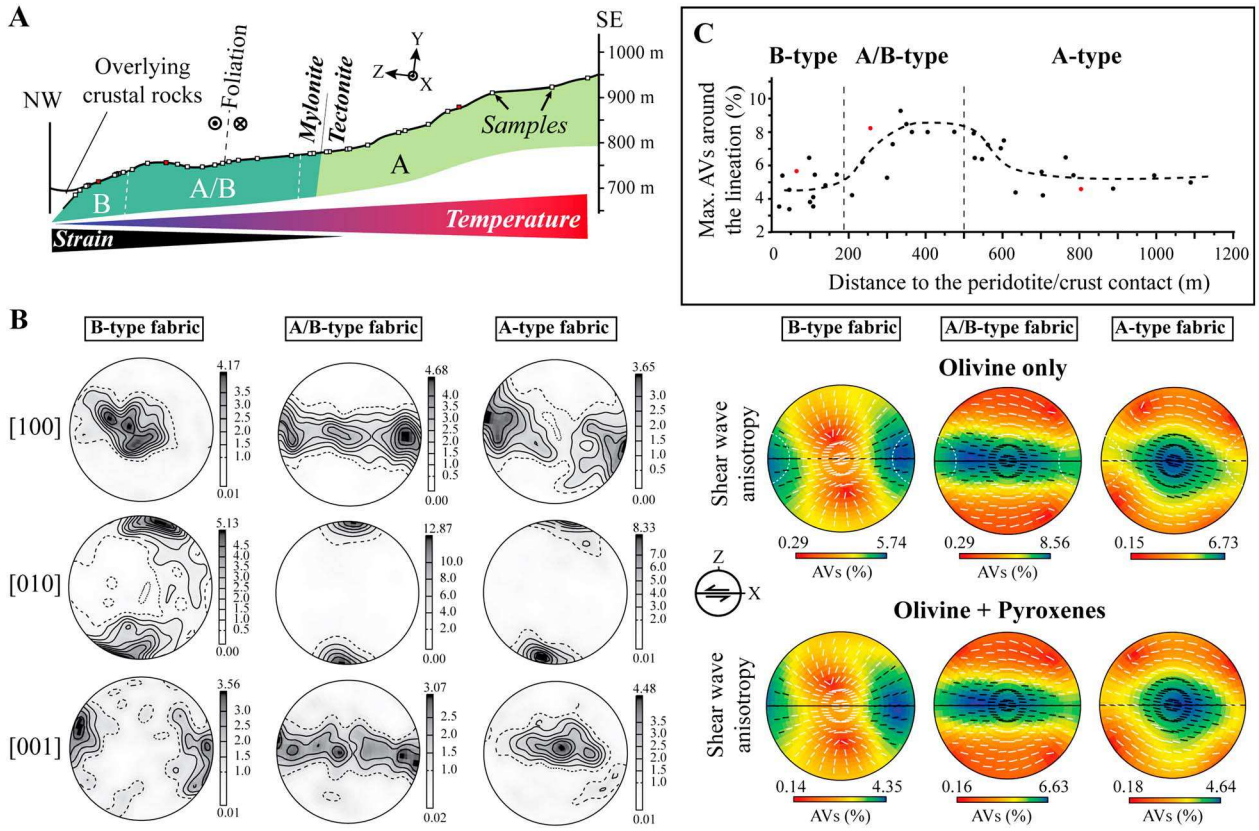

Figure 2. (a) Cross section of the Ronda shear zone (location in Figure 1) and location of the samples (squares). (b) Olivine lattice-preferred orientation (LPO) and shear wave anisotropy (AVs) with fast directions for three selected samples of peridotite across the shear zone (red squares), respectively, for the A-, A/B-, and B-type fabric domains. The LPO and AVs for the rest of the samples (white squares) are shown in *Précigout and Hirth* [2014] and in the supporting information, respectively. We calculated both AVs from olivine LPO only and from olivine + pyroxene LPOs based on modal compositions (pyroxene LPOs and modal contents are available in *Précigout and Hirth* [2014]). The LPOs and shear wave anisotropies are plotted in lower hemisphere equal-area pole figures with respect to the structural orientations *x* (lineation), *y* (normal to lineation in the foliation plane), and *z* (foliation pole). The LPOs have been collected using electron backscatter diffraction analyses on thin section considering one measurement per grain [see *Précigout and Hirth*, 2014]. They are shown for the three orthorhombic axes (100, 010, and 001) with isocontours and grey shading that represent multiples of uniform distribution. The shear wave anisotropies were calculated using the CareWare software of *Mainprice* [1990] available at http://www.gm.univ-montp2.fr/PERSO/mainprice/W_data/CareWare_Unicef_Programs/. The AVs pole figures show the difference of shear wave velocity (color shading in percent) between slow and fast components ($AVs = 200(Vs_1 - Vs_2)/(Vs_1 + Vs_2)$). Whereas A-type and B-type fabrics develop one maximum of shear wave anisotropy, respectively, normal and parallel to the lineation, the A/B-type fabric generates a girdled pattern with high AVs in the foliation plane. (c) Distribution of maximum shear wave anisotropy for olivine across the Ronda shear zone. Each sample is plotted with respect to its distance from the peridotite/crust contact [see *Précigout and Hirth*, 2014] and considering a 20° solid angle around the lineation (*x* AVs). We assume a solid angle of 20° to account for the obliquities induced by simple shear deformation and the natural variability of fabric pattern. The red dots are the selected samples shown in Figures 2a and 2b. The highest anisotropy (AVs = 8–9%) occurs in the A/B-type fabric domain.

increasing strain and decreasing temperature, and it results from changing olivine deformation mechanism from dominant dislocation creep in the tectonite to dominant grain boundary sliding (GBS) in the uppermost mylonite. Such a transition, in terms of mineral fabric and deformation mechanism, is expected to occur in the mantle wedge from the inner, high-temperature core to the outer, low-temperature rim beneath the overriding plate or above the subducting slab [*Kneller et al.*, 2008, and references therein]. The Ronda peridotite therefore provides a unique opportunity to investigate the relationships between olivine fabrics and shear wave splitting in the mantle wedge of subduction zones.

4. Shear Wave Splitting

In Figure 2b, we show the calculated shear wave anisotropy for A-, A/B-, and B-type fabrics with respect to the structural directions *x* (lineation) and *z* (foliation pole) (refer to the supporting information for further data). For both A-type and B-type fabrics, maximum AVs lies in the foliation plane but normal to the lineation for A-type fabric and parallel to lineation for B-type fabric. At high angle to foliation, A- and B-type fabrics

develop orthogonally polarized fast directions with respect to each other (white lines in Figure 2b). This effect has been proposed to account for the pattern of orthogonal fast directions observed across the volcanic arc of NE Japan [*Nakajima and Hasegawa*, 2004]. Between the A- and B-type fabrics, the A/B-type fabric develops high AV*s* through the whole foliation plane with maxima located roughly at 45° to lineation. Unlike the patterns of *S* wave anisotropy for A- and B-type fabrics, this transitional pattern implies a high shear wave splitting in the lineation direction, i.e., in the direction of the flow. To emphasize this, we show in Figure 2c the development of the maximum AV*s* across the shear zone around the lineation, i.e., within a solid angle of 20° to account for both the obliquity induced by simple shear deformation between the foliation plane and the olivine (010) plane and the natural variability in LPO pattern. We considered in this graph the AV*s* for olivine only. From the tectonite to upper mylonite, the maximum AV*s* along the *x* axis (*x* AV*s*) varies from ~5% to >8%, with the highest anisotropy forming a plateau in the region of A/B-type fabric. Both A- and B-type fabric domains show maximum *x* AV*s* lower than 6%. Concerning the effect of pyroxenes for shear wave splitting in Ronda (pyroxene LPOs and modal compositions are available in *Précigout and Hirth* [2014]), it does not change the AV*s* pattern, but it decreases the anisotropy for all of the fabric types, especially because the pyroxenes show a very weak fabric across the Ronda shear zone (Figure 2b) [*Précigout and Hirth*, 2014].

5. Discussion

The occurrence of "A-type to B-type" fabric transition with decreasing temperature across the Ronda shear zone indicates that such a fabric transition occurs in the mantle wedge of the subduction zone. The maximum temperature for the occurrence of B-type fabric has been estimated around 800°C based on experimental and numerical data sets [*Katayama and Karato*, 2006; *Kneller et al*., 2008]. B-type olivine fabric has been moreover reported from several peridotite massifs in subduction setting [*Mizukami et al*., 2004; *Skemer et al*., 2006]. In Ronda, the presence of B-type fabric in the uppermost/coldest part of the shear zone supports these features; syntectonic temperature has been documented around 850°C in the center mylonite [*Van der Wal and Vissers*, 1993]. Thus, the B-type fabric type cannot be ignored in the low-temperature mantle wedge of the subduction zones. However, as already documented for experimentally and naturally deformed olivine, we confirm that B-type fabric is weakly anisotropic (3–6%), and hence, it cannot account for shear wave splitting in high-delay-time subduction zones where a minimum of 8% AV*s* is required [*Kneller et al*., 2008; *McCormack et al*., 2013]. As an alternative, we highlight transitional A/B-type fabric for which olivine shear wave anisotropy can achieve more than 9% AV*s* with a mean AV*s* around 8% (Figure 2). Although the presence of pyroxenes may yield lower AV*s*, this fabric type has been documented in subduction xenoliths with more than 8% AV*s* considering both olivine and pyroxenes (Petit-Spots Volcanoes) [*Hiragane et al*., 2011]. *Hiragane et al*. [2011] moreover estimated temperature conditions for A/B-type samples between 800 and 1100°C based on petrological features, supporting the occurrence of high-AV*s*, A/B-type fabric at intermediate temperature of the lithospheric mantle. The A/B-type fabric thus provides a very good candidate to account for shear wave splitting in the subduction zones.

In Figure 3, we compare our natural data set from Ronda with the predicted thermal and deformational structures of the Ryukyu and Honshu subduction wedges, as well as to the *S* wave raypaths calculated from seismic stations in these two regions. We have chosen as examples both Ryukyu and Honshu because (1) they are "ideal" cases of subduction zone as they show trench-normal plate convergence and close to constant slab dip; (2) they record significant differences in average delay times, ~0.1–0.2 s in Honshu and ~1–2 s in Ryukyu [*Katayama et al*., 2009, and references therein]; and (3) large seismic shear wave data sets are available for both of them [*Peacock and Wang*, 1999; *Nakajima and Hasegawa*, 2004; *Long and Van der Hilst*, 2006; *Kneller et al*., 2005, 2008]. Following the modeled foliation tracks and considering A/B-type fabric as dominant between the isotherms 800 and 1000°C (1000°C represents a minimum value for the upper bound), we find that raypaths are tangent to the foliation throughout a major portion of the mantle wedge where A/B-type fabric occurs, i.e., in conditions that imply around 8% shear wave anisotropy (Figure 3a). At lower temperature, the seismic raypaths also crosscut a significant part of B-type fabric, but because of lower foliation dip, the shear wave anisotropy reduces to around 4% (Figure 3a). We then provide estimations of the delay times arising from the olivine fabric for different depths of earthquakes and considering the LPO-induced AV*s* all along the raypaths. The delay times were calculated for both "olivine only" and "olivine + pyroxenes" samples, addressing two cases of raypaths: the first one with raypaths parallel to the mantle flow, i.e., normal to the trench, and a second one at 30° of the flow direction in the mantle wedge (Figure 3). While seismic raypaths from deep earthquakes indicate more than 2 s of delay times, the ones from shallower

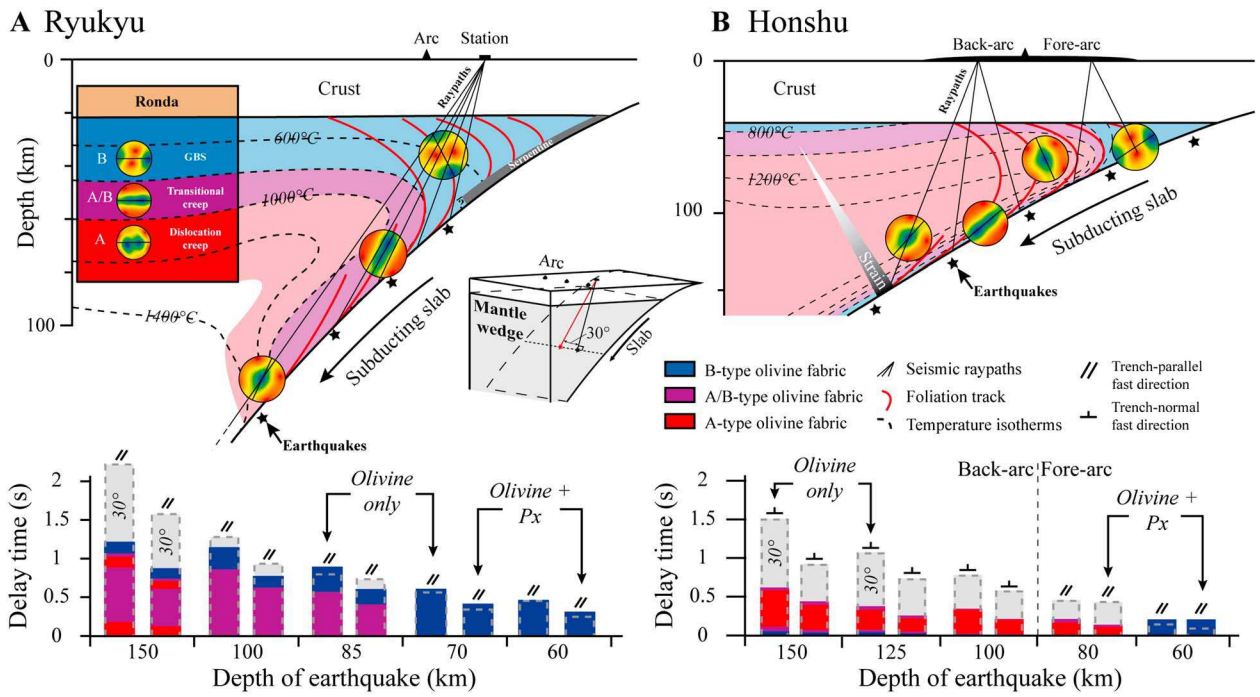

Figure 3. Application of the Ronda-based olivine fabric to shear wave anisotropy in the Ryukyu and Honshu subduction wedges. (a) Cross section of the subduction wedge in Ryukyu, including the isotherms, foliation tracks, and seismic raypaths [*Long and Van der Hilst*, 2006; *Kneller et al*., 2008]. Using the AVs patterns from Ronda and considering transitional A/B-type olivine fabric between the isotherms 800 and 1000°C because of changing deformation mechanisms from dominant GBS to dislocation creep, we estimate the delay times for the five cases of seismic raypaths that originate from different depths (bar graph). For each depth, we consider one raypath normal to the trench and a second one at 30° obliquity of the slab dip (3-D sketch and grey bars). For the trench-normal raypaths, we show how each fabric type contributes to the delay time (color coding). Delay times are also shown considering both olivine LPO only and olivine + pyroxene (Px) LPOs. Whereas low delay times arise from B-type fabric, high delay times are mostly due to A/B-type fabric. In both cases, these natural AVs involve trench-parallel fast directions with delay times ranging between 0.5 and 2 s, as observed in Ryukyu (see text). (b) Cross section and delay time estimations (bar graph) for the Honshu subduction system. Temperature isotherms and seismic raypaths are from *Kneller et al*. [2005] and *Nakajima and Hasegawa* [2004], respectively. The foliation tracks are predicted based on the study of *Kneller et al*. [2008]. In this case, only A- and B-type fabrics significantly contribute to the delay times, which range from $<$0.1 to 1.5 s. The high obliquity between the raypaths and foliation tracks also involves a switch from trench-parallel to trench-normal fast directions, as shown in Honshu [*Nakajima and Hasegawa*, 2004]. However, although olivine AVs accounts for the delay times recorded in Honshu, delay times are generally overestimated in the back-arc regions.

earthquakes that only go through the B-type fabric domain show delay times around 0.5 s. This range of delay times is typical of the Ryukyu subduction system [*Long and Van der Hilst*, 2006; *Katayama et al*., 2009]. The expected position of olivine LPOs in the mantle wedge—based on the foliation tracks—moreover involves trench-parallel fast splitting direction for all of the raypaths involved. Our calculations indicate nonetheless that 8% AVs is required to achieve delay times of 2 s, as recently concluded [*McCormack et al*., 2013]. Considering the additional effect of pyroxenes, AVs is lower than 8%, and the predicted delay times are far below 2 s for the longest raypaths, even for oblique raypaths at 30° (Figure 3a).

In contrast to Ryukyu, the seismic stations in the Honshu peninsula have recorded very small delay times, ranging from 0 to 0.6 s [*Nakajima and Hasegawa*, 2004]. In this subduction system, the slab dips at around 30°—instead of 50° in the case of Ryukyu—and hence, most of the raypaths are significantly oblique to the foliation (Figure 3b). As a consequence, the LPO patterns from Ronda involve significantly lower shear wave anisotropy for A-, A/B-, and B-type fabric domains. Furthermore, our calculations for Honshu predict that delay times mostly originate from A- and B-type fabrics; the contribution from the A/B-type fabric is minor (Figure 3b). This feature implies very low delay times—especially for oblique raypaths in the B-type fabric domain—and trench-parallel fast directions for shallow earthquakes, whose seismic raypaths are recorded in the fore-arc region. In contrast, we predict trench-normal fast directions and high delay times for deeper earthquakes recorded in the back-arc region ($>>$0.5 s) (Figure 3b). These back-arc delay times do no match the ones documented in Honshu, even if we consider the effect of pyroxenes, and thus we probably overestimate the shear wave anisotropy that arises from the back-arc mantle. The presence of a strain gradient in the mantle wedge may account for this discrepancy. Indeed, while we expect very high strain

deformation in the supraslab mantle wedge, strain should significantly decrease away from the slab beneath the overriding plate. Experimental and numerical data have shown that because of dislocation creep, higher finite strain increases the degree of mineral alignment—or fabric strength [*Tommasi et al*., 2000; *Bystricky et al*., 2000; *Hansen et al*., 2014]—which is the first-order parameter that controls shear wave anisotropy [*Mainprice*, 1990]. Thus, in regions dominated by dislocation creep (A- and A/B-type fabrics), such a strain gradient may have a direct impact on shear wave anisotropy, which would be higher in the supraslab mantle (Figure 3b). Echoing the conclusions of *Katayama* [2009] and *Hacker and Abers* [2012], we therefore suggest that most of the seismic anisotropy occurs in the supraslab mantle wedge because of strain-induced fabric anisotropy in Honshu and more probably Ryukyu as well.

Recent modeling of a seismic data set suggests that an ~1 km thick layer with 8% AV*s* occurs above the subducting slab in Ryukyu [*McCormack et al*., 2013]. This layer is considered to be sandwiched between an underlying supraslab layer with 10% AV*s* and an overlying wedge with 4% AV*s*. In the case of both domains of 8% and 4% AV*s*, our documentation confirms the relevance of the transitional A/B-type fabric to account for the seismic anisotropy of the Ryukyu subduction wedge (Figure 3a). However, the Ronda transitional fabric does not match the thin layer of 10% AV*s* immediately above the subducting slab. Previous studies have proposed the occurrence of serpentinite layers above the subducting slab, which would be highly anisotropic (i.e., $\geq$10% AV*s*) [*Katayama et al*., 2009; *McCormack et al*., 2013], but an inherent problem with this explanation arises because temperatures at the intersection between the seismic raypaths and supraslab mantle are always higher than the breakdown temperature for serpentine (~700°C) [*Ulmer and Trommsdorff*, 1995; *Peacock*, 2001]. As concluded by *Kneller et al*. [2008], it is therefore unlikely that serpentine would be responsible for this high-AV*s* layer. As an alternative, we propose that A/B-type fabric can account for this feature considering higher finite strain above the subducting slab. In contrast to B-type fabric, which results from dominant GBS-controlled creep, i.e., diffusion creep [*Sundberg and Cooper*, 2008] or disGBS [*Précigout et al*., 2007], A/B-type fabric results from a significant component of dislocation creep [*Précigout and Hirth*, 2014], and hence, we might expect stronger LPO because of higher finite strain in close proximity to the subducting slab. As a consequence, the seismic anisotropy for A/B-type fabric would be higher, potentially accounting for the 10% AV*s* deduced from seismic models [*McCormack et al*., 2013]. The presence of such a high fabric anisotropy, i.e., strong LPO, above the subducting slab has also been recently proposed based on seismic features in Alaska [*Hacker and Abers*, 2012].

In part due to the paucity of data regarding natural olivine fabric at low mantle temperatures ($<$900°C), some recent studies have deemphasized olivine fabrics as source of high anisotropy in subduction zones [*Long and Silver*, 2008; *Katayama et al*., 2009]. Based on detailed documentation in the Ronda peridotite, and considering isotherms geometry and foliation tracks in the mantle wedges of the Ryukyu and Honshu subduction systems, we show that olivine LPOs can account for shear wave anisotropy because of transitional A/B-type olivine fabric between the 800 and 1000°C isotherms. Our findings provide a natural analogue of mantle wedge deformation and support the occurrence of an olivine fabric transition across the mantle wedge [*Karato et al*., 2008; *Kneller et al*., 2008; *Abt et al*., 2009; *McCormack et al*., 2013]. Nevertheless, both Ryukyu and Honshu represent ideal cases of subduction system, as they show trench-normal plate convergence and constant slab dip. These two features can significantly change depending on the subduction system [*Lallemand et al*., 2005; *Long and Silver*, 2008], and hence, there is not a straightforward relationship between the olivine LPO and shear wave splitting in the mantle wedge. We stress therefore that the thermal state of the mantle wedge, geometry of the subduction zone, and intensity of deformation need to be considered in future studies to properly account for the mantle LPO for shear wave splitting in subduction wedges.

Acknowledgments
We thank Jean-Pierre Burg (ETH Zürich, Switzerland), Frédéric Gueydan (Géosciences Montpellier, France), and Laurent Jolivet (IST Orléans, France) for reviewing the paper and for their fruitful discussions. We also thank Greg Hirth (Brown University, USA) for his help in funding the project. This project has been funded by the NSF award EAR-0738880, the ETH Zürich (ETH postdoctoral fellowship FEL 01 09-3), and the ERC RHEOLITH (grant 290864). B.S.G.A. acknowledges financial support from the Swedish Research Council, grant 2012-4449. The data set used in this study is available at http://www.sciencedirect.com/science/article/pii/S0012821X14002040.

The Editor thanks Bradley Hacker and an anonymous reviewer for their assistance in evaluating this paper.

References

Abt, D. L., K. M. Fisher, G. A. Abers, W. Strauch, J. M. Protti, and V. Gonzalez (2009), Shear wave anisotropy beneath Nicaragua and Costa Rica: Implications for flow in the mantle wedge, *Geochem. Geophys. Geosyst.*, *10*, Q05S15, doi:10.1029/2009GC002375.

Balanyá, J. C., V. García-Dueñas, and J. M. Azañon (1997), Alternating contractional and extentional events in the Alpujarride nappes of the Alboran Domain (Betics, Gibraltar Arc), *Tectonics*, *16*(2), 226–238, doi:10.1029/96TC03871.

Behn, M. D., G. Hirth, and P. B. Kelemen (2007), Trench-parallel anisotropy produced by foundering of arc lower crust, *Science*, *317*, 108–110, doi:10.1126/science.1141269.

Bystricky, M., K. Kunze, L. Burlini, and J.-P. Burg (2000), High shear strain of olivine aggregates: Rheological and seismic consequences, *Science*, *290*, 1564–1567, doi:10.1126/science.290.5496.1564.

Faccenda, M., L. Burlini, T. V. Gerya, and D. Mainprice (2008), Fault-induced seismic anisotropy by hydration in subducting oceanic plates, *Nature*, *455*, 1097–1100, doi:10.1038/nature07376.

Garrido, C. J., F. Gueydan, G. Booth-Rea, J. Précigout, K. Hidas, J. A. Padron-Navarta, and C. Marchesi (2011), Garnet Lherzolites and Garnet-spinel mylonites in the Ronda Peridotite: Vestiges of Oligocene Back-arc mantle lithospheric extension in the Western Mediterranean, *Geology*, *39*(10), 927–930, doi:10.1130/G31760.1.

Hacker, B. R., and G. A. Abers (2012), Subduction Factory 5: Unusaully low Poisson's ratios in subduction zones from elastic anisotropy of peridotite, *J. Geophys. Res.*, *117*, B06308, doi:10.1029/2012JB009187.

Hansen, L. N., Y.-H. Zhao, M. E. Zimmerman, and L. Kohlstedt (2014), Protracted fabric evolution in olivine: Implications for the relationship among strain, crystallographic fabric, and seismic anisotropy, *Earth Planet. Sci. Lett.*, *387*, 157–168, doi:10.1016/j.epsl.2013.11.009.

Hiragane, Y., T. Mizukami, T. Morishita, K. Michibayashi, N. Abe, and N. Hirano (2011), Direct evidence for upper mantle structure in the NW Pacific Plate: Microstructural analysis of a petit-spot peridotite xenolith, *Earth Planet. Sci. Lett.*, *302*, 194–202, doi:10.1016/j.epsl.2010.12.011.

Jung, H., and S.-I. Karato (2001), Water-induced fabric transitions in olivine, *Science*, *293*, 1460–1463.

Karato, J.-I., H. Jung, I. Katayama, and P. Skemer (2008), Geodynamic significance of seismic anisotropy of the upper mantle: New insights from laboratory studies, *Annu. Rev. Earth Planet. Sci.*, *36*, 59–95, doi:10.1146/annurev.earth.36.031207.124120.

Katayama, I. (2009), Thin anisotropic layer in the mantle wedge beneath northeast Japan, *Geology*, *37*, 211–214, doi:10.1130/G25413A.1.

Katayama, I., and S.-I. Karato (2006), Effect of temperature on the B- to C-type olivine fabric transition and implication for flow pattern in subduction zones, *Phys. Earth Planet. Inter.*, *157*, 33–45, doi:10.1016/j.pepi.2006.03.005.

Katayama, I., K. I. Hirauchi, K. Michibayashi, and J.-I. Ando (2009), Trench-parallel anisotropy produced by serpentine deformation in the hydrated mantle wedge, *Nature*, *461*, 1114–1118.

Kneller, E. A., P. E. van Keken, S.-I. Karato, and J. Park (2005), B-type olivine fabric in the mantle wedge: Insights from high-resolution non-Newtonian subduction zone models, *Earth Planet. Sci. Lett.*, *237*, 781–797, doi:10.1016/j.epsl.2005.06.049.

Kneller, E. A., M. D. Long, and P. E. Van Keken (2008), Olivine fabric transitions and shear wave anisotropy in the Ryukyu subduction system, *Earth Planet. Sci. Lett.*, *268*, 268–282, doi:10.1016/j.epsl.2008.01.004.

Lallemand, S., A. Heuret, and D. Boutelier (2005), On the relationships between slab dip, back-arc stress, upper plate absolute motion, and crustal nature in subduction zones, *Geochem. Geophys. Geosyst.*, *6*, Q09006, doi:10.1029/2005GC000917.

Lenoir, X., C. J. Garrido, J.-L. Bodinier, J.-M. Dautria, and F. Gervilla (2001), The recrystallization front of the Ronda Peridotite: Evidence for melting and thermal erosion of subcontinental lithospheric mantle beneath the Alboran Basin, *J. Petrol.*, *42*(1), 141–158, doi:10.1093/petrology/42.1.141.

Long, M. D., and P. G. Silver (2008), The subduction zone flow field from seismic anisotropy: A global view, *Science*, *319*, 315–318.

Long, M. D., and R. D. Van der Hilst (2006), Shear wave splitting from local events beneath the Ryukyu arc: Trench-parallel anisotropy in the mantle wedge, *Phys. Earth Planet. Int.*, *155*, 300–312, doi:10.1016/j.pepi.2006.01.003.

Mainprice, D. (1990), An efficient fortran program to calculate seismic anisotropy from the lattice preferred orientation of minerals, *Comput. Geosci.*, *16*, 385–393.

McCormack, K., E. A. Wirth, and M. D. Long (2013), B-type olivine fabric and mantle wedge serpentinization beneath the Ryukyu arc, *Geophys. Res. Lett.*, *40*, 1697–1702, doi:10.1002/grl.50369.

Mizukami, T., S. R. Wallis, and J. Yamamoto (2004), Natural examples of olivine lattice preferred orientation patterns with a flow-normal a-axis maximum, *Nature*, *427*, 432–436, doi:10.1038/nature02233.

Nakajima, J., and A. Hasegawa (2004), Shear-wave polarization anisotropy and subduction-induced flow in the mantle wedge of northeastern Japan, *Earth Planet. Sci. Lett.*, *225*, 365–377, doi:10.1016/j.epsl.2004.06.011.

Peacock, S. M. (2001), Are the lower planes of double seismic zones caused by serpentine dehydration in subducting oceanic mantle?, *Geology*, *29*(4), 299–302, doi:10.1130/0091-7613(2001).

Peacock, S. M., and K. Wang (1999), Seismic consequences of warm versus cool subduction metamorphism: Examples from Southwest and Northeast Japan, *Science*, *286*, 937–939, doi:10.1126/science.286.5441.937.

Précigout, J., and G. Hirth (2014), B-type olivine fabric induced by grain boundary sliding, *Earth Planet. Sci. Lett.*, *395*, 231–240, doi:10.1016/j.epsl.2014.03.052.

Précigout, J., F. Gueydan, D. Gapais, C. J. Garrido, and A. Essaifi (2007), Strain localisation in the subcontinental mantle - a ductile alternative to the brittle mantle, *Tectonophysics*, *445*, 318–336, doi:10.1016/j.tecto.2007.09.002.

Précigout, J., F. Gueydan, C. J. Garrido, N. Cogné, and G. Booth-Rea (2013), Deformation and exhumation of the Ronda peridotite (Spain), *Tectonics*, *32*, 1011–1025, doi:10.1002/tect.20062.

Silver, P., D. Mainprice, W. B. Ismaïl, A. Tommasi, and G. Barruol (1999), Mantle structural geology from seismic anisotropy, in *Mantle Petrology: Field Observations and High Pressure Experimentations: A Tribute to Francis, R. (Joe) Boyd: The Geochemical Society*, *Spec. Publ.*, vol. 6, edited by Y. Fei, C. M. Bertka, and B. O. Mysen, pp. 79–103, The Geochemical Society, Houston, Tex.

Skemer, P., I. Katayama, and S.-I. Karato (2006), Deformation fabrics of the Cima di Gagnone peridotite massif, Central Alps, Switzerland: Evidence of deformation at low temperatures in the presence of water, *Contrib. Mineral. Petrol.*, *152*, 43–51, doi:10.1007/s00410-006-0093-4.

Sundberg, M., and R. F. Cooper (2008), Crystallographic preferred orientation produced by diffusional creep of harzburgite: Effects of chemical interactions among phases during plastic flow, *J. Geophys. Res.*, *113*, B12208, doi:10.1029/2008JB005618.

Tasaka, M., K. Michibayashi, and D. Mainprice (2008), B-type olivine fabrics developed in the fore-arc side of the mantle wedge along a subducting slab, *Earth Planet. Sci. Lett.*, *272*, 747–757, doi:10.1016/j.epsl.2008.06.014.

Tommasi, A., D. Mainprice, G. Canova, and Y. Chastel (2000), Viscoplastic self-consistent and equilibrium-based modeling of olivine lattice preferred orientations: Implications for the upper mantle seismic anisotropy, *J. Geophys. Res.*, *105*(B4), 7893–7908, doi:10.1029/1999JB900411.

Ulmer, P., and V. Trommsdorff (1995), Serpentine stability to mantle depths and subduction-related magmatism, *Science*, *268*, 858–861.

Van der Wal, D., and R. L. M. Vissers (1993), Uplift and emplacement of upper mantle rocks in the western Mediterranean, *Geology*, *21*, 1119–1122.

Van der Wal, D., and R. L. M. Vissers (1996), Structural petrology of the Ronda Peridotite, SW Spain: Deformation history, *J. Petrol.*, *37*(1), 23–43.

Vauchez, A., and C. J. Garrido (2001), Seismic properties of an asthenospherized lithospheric mantle: Constraints from lattice preferred orientations in peridotite from the Ronda massif, *Earth Planet. Sci. Lett.*, *192*, 235–249, doi:10.1016/S0012-821X(01)00448-4.